Soft X-ray tomography of phenotypic switching and the cellular response to antifungal peptoids in *Candida albicans*

Maho Uchida[a], Gerry McDermott[a], Modi Wetzler[b], Mark A. Le Gros[c], Markko Myllys[a,d], Christian Knoechel[a], Annelise E. Barron[b], and Carolyn A. Larabell[a,c,1]

[a]Department of Anatomy, School of Medicine, University of California, San Francisco, CA; [b]Bioengineering Department, Stanford University, Palo Alto, CA; [c]Physical Biosciences Division, Lawrence Berkeley National Laboratory, Berkeley, CA; and [d]Department of Physics, University of Jyväskylä, Finland

Edited by John Kuriyan, University of California, Berkeley, CA, and approved September 23, 2009 (received for review June 4, 2009)

The opportunistic pathogen *Candida albicans* can undergo phenotypic switching between a benign, unicellular phenotype and an invasive, multicellular form that causes candidiasis. Increasingly, strains of *Candida* are becoming resistant to antifungal drugs, making the treatment of candidiasis difficult, especially in immunocompromised or critically ill patients. Consequently, there is a pressing need to develop new drugs that circumvent fungal drug-resistance mechanisms. In this work we used soft X-ray tomography to image the subcellular changes that occur as a consequence of both phenotypic switching and of treating *C. albicans* with antifungal peptoids, a class of candidate therapeutics unaffected by drug resistance mechanisms. Peptoid treatment suppressed formation of the pathogenic hyphal phenotype and resulted in striking changes in cell and organelle morphology, most dramatically in the nucleus and nucleolus, and in the number, size, and location of lipidic bodies. In particular, peptoid treatment was seen to cause the inclusion of lipidic bodies into the nucleus.

Candida albicans is a common component of the human commensal flora, and is estimated to be present in the gastrointestinal and genitourinary tract of 80% of the population. In response to a range of environmental and/or cellular cues, *C. albicans* can switch from a benign yeast-like phenotype to a highly invasive, multicellular pathogenic cell type by the formation of hyphae (Fig. 1) (1). The hyphal phenotype is responsible for the mycosis candidiasis (2). In most instances, candidiasis is a minor, superficial condition that can be treated readily. However, as with most fungal pathogens, *C. albicans* is becoming increasingly resistant to antifungal drugs (3, 4), making it difficult to treat otherwise relatively simple infections. The situation is much worse in the case of critically ill or immunocompromised individuals where candidiasis can become systemic. Such systemic infections can have devastating consequences and a mortality rate of 40% (3–7). Consequently, there is now a pressing need to develop safe, effective antifungal drugs that can circumvent both innate and acquired drug-resistance mechanisms. To date, developing new pharmaceuticals has typically relied on designing or discovering molecules capable of perturbing the function of a single gene, protein, or molecular event thought to be involved in the aetiology of a disease (8). Taking such a highly targeted approach is thought to be one of the main failings in the drug discovery model, and is considered to be one of the factors that have lead to a shortage of new drugs entering the clinic (9). It has been proposed that a more productive approach to drug discovery is to identify, test, and visualize potential therapeutic molecules directly in the complexity of an entire, fully functional biological system, i.e., in the milieu of a cell (8, 10). Recently, soft X-ray tomography has been developed as an imaging modality well suited to this type of study, especially since it can be used to image the sub-cellular structure of large numbers of cells (11–16). In the work described here, we used soft X-ray tomography to image changes that take place in the subcellular organization of *C. albicans* as a consequence of phenotypic switching. We then applied the same methods to imaging *C. albicans* cells that had been treated with antifungal peptoids, a class of peptidomimetics with potential to be developed as antifungal drugs that circumvent microbial drug-resistance mechanisms.

Soft X-ray tomography stands alone as a technique for imaging eukaryotic cells. No other high-resolution imaging modality is capable of quantitatively imaging the subcellular organization of fully hydrated cells in excess of 10 μm thick (12–14). Currently, XM-2, the X-ray microscope used in this work, is capable of imaging biological specimens with a spatial resolution of 50 nm. In the near future, incorporation of the latest generation of zone plate optics into this microscope will increase the achievable spatial resolution to better than 15-nm resolution (17). In soft X-ray tomography, the image contrast is generated by the differential, quantitative absorption of X-ray photons. Therefore, cells do not need to be treated with contrast-enhancing chemicals, or subjected to other procedures that could potentially disrupt or even destroy the native cellular structure before imaging. Instead, cells are simply taken from their growth chamber and cryo-immobilized (13). The illuminating photons used in soft X-ray tomography have energies that fall within a region of the electromagnetic spectrum known as the "water window." In this spectral range, water is an order of magnitude more transmissive than carbon and nitrogen (18). Because this absorption follows Beer's Law, the absorption of photons is linear and a function of the biochemical composition at each point in the cell (13, 19). Organelles and other subcellular structures of interest are readily identifiable and can be segmented (i.e., isolated from the rest of the cell) based on their X-ray absorption characteristics (12–14, 19). Soft X-ray tomography is a relatively high-throughput imaging technique; it takes $<$3 min to collect projection images necessary for calculation of a tomographic reconstruction (plus, each field of view is sufficiently large that it may contain more than one cell, in the case of yeast-like *C. albicans*, we imaged three to five cells per dataset).

Antimicrobial peptides (AMPs) are widely produced by most members of the plant and animal kingdoms, including humans, as a first line of defense against microbial infection (20). AMPs exhibit broad-spectrum activity against many pathogens, and function by mechanisms to which microbes have failed to develop resistance (20, 21). These characteristics make AMPs ideal

Author contributions: M.U., G.M., M.A.L.G., and C.A.L. designed research; M.U., G.M., M.W., M.A.L.G., and C.K. performed research; M.W. and A.E.B. designed and synthesized peptoids; M.M. developed analytical software; M.U., M.W., and M.M. analyzed data; and M.U., G.M., M.W., M.A.L.G., and C.A.L. wrote the paper.

The authors declare no conflict of interest.

This article is a PNAS Direct Submission.

[1]To whom correspondence should be addressed. E-mail: carolyn.larabell@ucsf.edu.

This article contains supporting information online at www.pnas.org/cgi/content/full/0906145106/DCSupplemental.

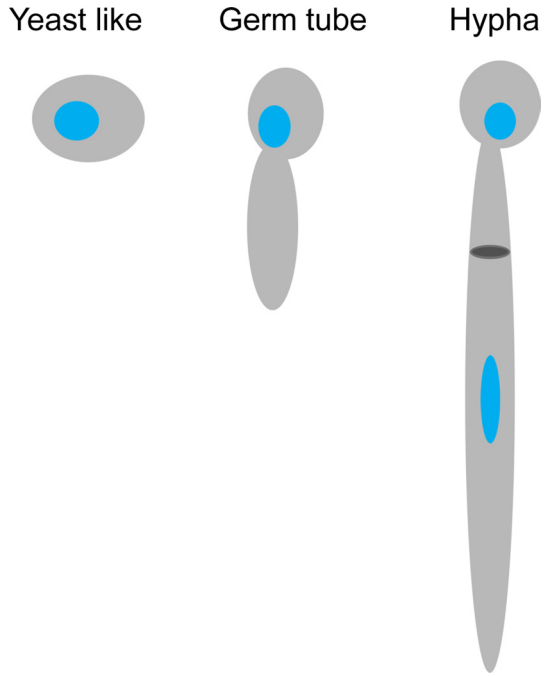

Fig. 1. Schematic representation of the three phenotypes adopted by *C. albicans*. Blue, nucleus; dark gray, septum.

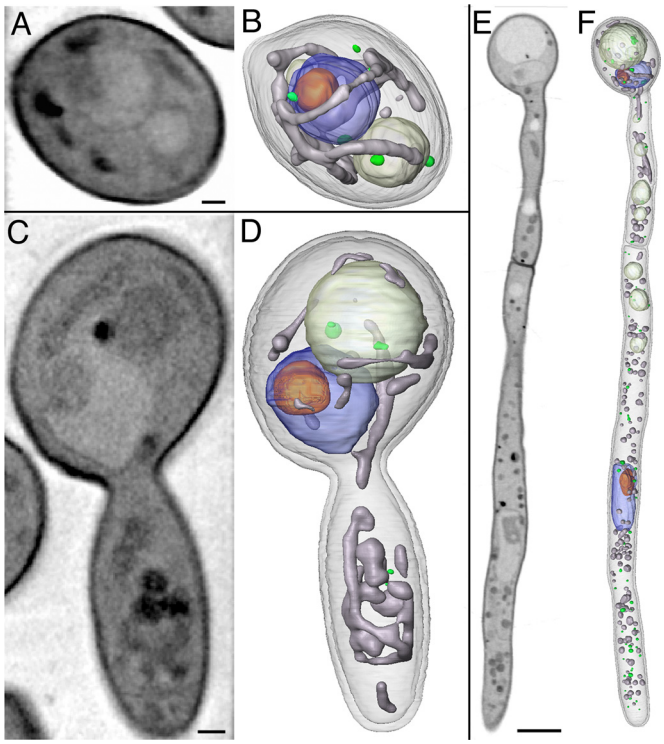

Fig. 2. Soft X-ray tomographic reconstruction of phenotypically distinct *C. albicans* cells. A representative orthoslice from each tomographic reconstruction is shown for a yeast-like (*A*), germ-tube (*C*) and hyphal (*E*) cell. Volume rendered views of the same cells are shown in (*B*, *D*, and *F*) respectively showing selected organelles that have been segmented and color-coded for identification. Blue, nucleus; orange, nucleolus; gray, mitochondria; yellow, vacuole; green, lipid bodies. (Scale bar for *A–D*, 0.5 μm, for *E* and *F*, 2.0 μm.)

candidates for development as drug molecules. Unfortunately, AMPs are prone to rapid proteolysis in vivo; thus, hindering their clinical applications (22). However, peptoids, a class of peptidomimetics (23), are extremely resistant to proteolysis (24), and possess broad-spectrum antimicrobial activity against many pathogenic organisms, including *C. albicans* (25). Consequently, peptoids are a much more attractive system for studying and developing novel antimicrobial and antifungal therapies. In this study, we treated *C. albicans* with two peptoids, termed peptoid 1 and peptoid 2 (Fig. S1), and imaged the subcellular consequences.

Peptoid 1 was designed to mimic magainin 2, one of the most established and widely studied AMPs (26). Peptoid 2 was designed to have homology with a family of AMPs previously shown to have strong antifungal activity against *C. albicans* (27). The mode of action by which these peptoids function is the subject of ongoing debate, but the evidence indicates that peptoids likely function similar to AMPs. However, even in the case of the more studied AMPs, there are still a number of unanswered questions regarding the precise mechanism(s) by which they act. One of the most widely accepted views being that AMPs exert at least part of their effects through membrane disruption (28). For example, a family of AMPs with high structural similarity to peptoid 2 was reported to cause disruption of *C. albicans* membranes (27). Based on the activity of peptoid 1 in membrane-mimetic vesicles and monolayers, it is reasonable to expect it to also cause membrane disruption (25). However, magainin 2 has also been shown to damage DNA in yeast (29); thus, demonstrating that AMPs and peptoids may have both intracellular and intranuclear effects.

Results

We began this study by establishing the subcellular architecture of the three phenotypes displayed by *C. albicans*, namely, yeast-like, germ-tube, and hyphal cells. Live cells were mounted in thin-walled glass capillary tubes, cryo-immobilized, and then imaged by soft X-ray microscopy. A tomographic dataset for each was obtained by collecting projection images at 2° increments around a rotation axis. The projection data were then computationally reconstructed to give the 3D cell volumes, which were then segmented to isolate, visualize, and quantify organelles and other subcellular structures (Fig. 2; Movies S1–S3). For the pathogenic form of *C. albicans* cells (i.e., the hyphal cell shown in Fig. 2 *E* and *F* and Movies S3 and S4) with cell lengths greater than the microscope field of view, projection series were collected from sequentially overlapping fields of view. Each series was individually reconstructed and then computationally "stitched together" to form the single, seamless tomographic reconstructions shown in Fig. 2*E*. For smaller cells, such as the yeast-like or germ-tube cells, each field of view contained between one and four cells, each of which could be reconstructed and segmented. Consequently, significant numbers of cells could be imaged tomographically for each peptoid treatment.

Subcellular structures such as the nucleus, nucleolus, mitochondria, vacuole, and lipid bodies were segmented based on the calculated linear absorption coefficients (LAC) at each voxel (Table S1). The measured LAC value for each voxel is determined by the biochemical composition at that point in the cell. Regions of the cell with relatively similar biochemical composition (at the level of spatial resolution observed) have characteristic LAC values (13, 19). For example, structures such as lipid bodies have consistent LAC values within the same cell, between cells, and can even be consistent between different cell types. That said, within a particular organelle, such as a nucleus, the LAC values vary in accordance with the internal structures and molecular densities. In this work, it was possible to segment organelles on their measured LAC values alone, and subsequently, assign the identity based on LAC and organelle shape

Table 1. Phenotypes of peptoid treated cells

	Yeast like	Germ tube
Control	11	10
Peptoid 1	8	3
Peptoid 2	9	1

Total number of segmented cells are categorized by phenotype.

established by other modalities (in particular, light and electron microscopy (30–32)). In this regard, segmentation of organelles in a cell imaged by soft X-ray tomography is analogous to differentiating liver from kidney, fat from muscle, or normal from abnormal tissue, in a patient imaged using clinical computed axial tomography (CAT).

Initially, the reconstructed cells were manually segmented. However, the excellent signal-to-noise inherent in soft X-ray tomographic data allowed us to apply automated segmentation methods, and thus, greatly speed up this process. To check the accuracy of the automated method, we segmented cells that had previously been segmented manually. A comparison of organelle volumes showed that the automated methods produced values that were within 10% of those obtained by manual segmentation.

Overall, we found that cells with the germ-tube phenotype closely resembled those of yeast-like cells in terms of organelle organization and structures. A number of dense objects with average volume of 0.07 μm^3 were assigned as lipid droplets based on their average LAC values of 0.75 ± 0.09 μm^{-1} (for a list of segmented organelle LAC values, see Table S1). The mitochondria appeared as single, continuous branched structures that curved around the nucleus and the vacuole. The segmented hyphal cells showed marked structural differences compared with yeast-like and germ-tube phenotypes. The nuclei and nucleoli were less spherical, and much more elongated, and multiple small vacuoles were apparent, in particular in the region nearest the primary cell. There appeared to be no vacuoles close to the hyphal tip, or even in the lower half of the hyphal cell.

To determine the cellular consequences of antifungal peptoid treatment on *C. albicans* cells, we collected tomographic data on cells that had been incubated with two different peptoids, peptoids 1 and 2, at a concentration corresponding to a minimum inhibitory concentration (MIC) of 50% (Fig. S1 and Movies S5 and S6). Characteristic of treatment with either peptoid molecule was the inhibition of the hyphal phenotype. Of the peptoid 1 treated cells, 73% of cells had a yeast-like phenotype, with the other 27% having the germ-tube phenotype. However, 90% of peptoid 2 treated cells had the yeast-like phenotype, with the remainder having a germ-tube phenotype (Table 1). In all cases, peptoid treatment resulted in an increase in the size and number of lipid-like structures and changes in the structure of the nucleoli (Fig. 3). We compared the cell volumes, and the volumes of lipid-like structures, nuclei, and nucleoli, in peptoid treated cells with those of the control cells (Fig. 4). Although the volume of the nucleus differed between control and peptoid treated cells, no significant difference in the average volume of nucleus relative to the cell volumes was observed between control (6.4 ± 1.5%) and peptoid treated cells (peptoid 1: 6.1 ± 0.7%; peptoid 2: 6.4 ± 1.1%). However, the average volume of the nucleolus relative to the cell volumes was smaller in peptoid 2 treated cells (1.0 ± 0.5%) compared with that of the control (2.0 ± 0.4%) and peptoid 1 treated cells (1.6 ± 0.4%) (Fig. 4*A*). Interestingly, the average volume of lipids relative to the cell volumes in peptoid 2 treated cells (0.60 ± 0.4%) was significantly higher compared with those of the control (0.06 ± 0.03%) and peptoid 1 treated cells (0.12 ± 0.04%). When the volumes of lipidic bodies was compared between peptoids 1 and 2 treated cells, the average percentage volume of lipids in peptoid 2 treated cells was 80% higher than that of peptoid 1 treated cells (Fig. 4*B*). In addition, deformation of vacuoles was observed in peptoid 1 treated cells (Fig. 3*D*). We also observed unexpected large structures em-

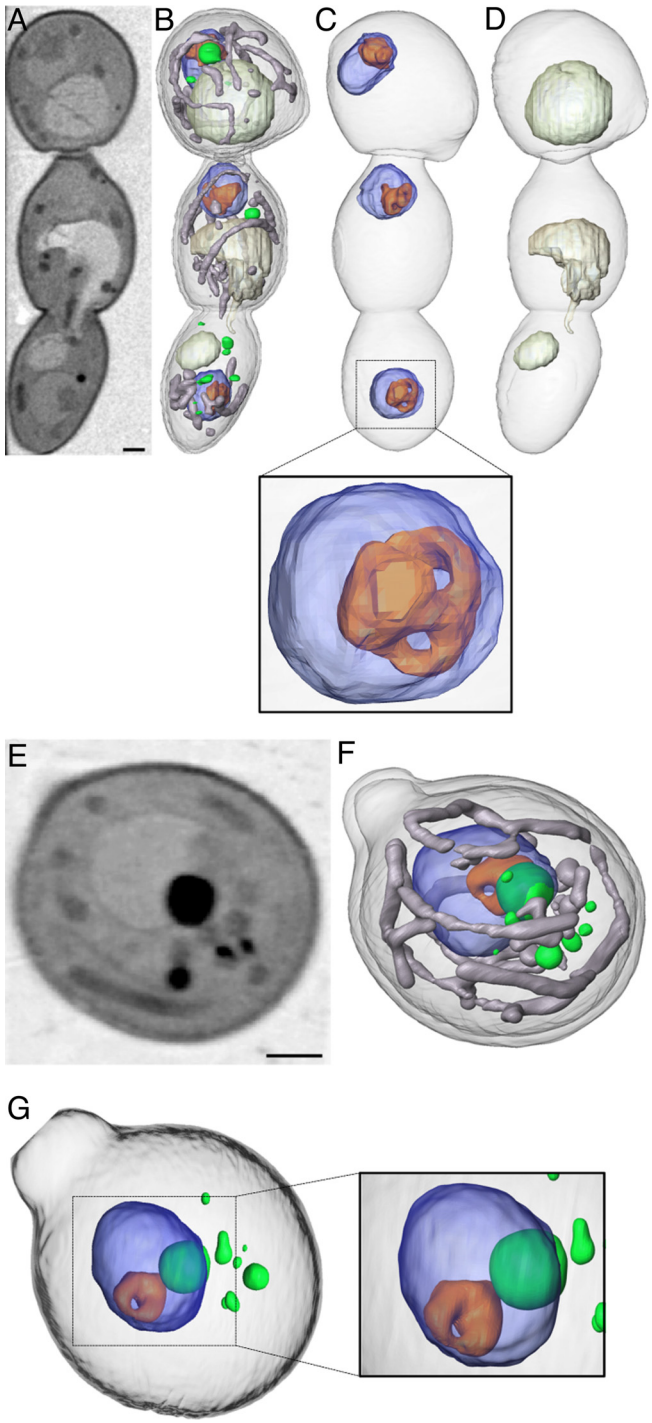

Fig. 3. Soft X-ray tomography of *C. albicans* cells after treatment with peptides. Peptoid 1 treated cell (*A–D*) Representative orthoslice through the tomographic reconstruction (*A*). All segmented organelles (*B*). Segmented nucleus and nucleolus (*C*). Peptoid 1 induced structural changes in the nucleolus are shown in detail in the *Inset*. Segmented vacuoles (*D*). Peptoid 2 treated cell (*E–G*). Representative orthoslice through the tomographic reconstruction (*E*). All segmented organelles (*F*). Segmented nucleus, nucleolus and lipid bodies (*G*). Peptoid 2 induced structural changes in the nucleolus and the incorporation of a large lipid body into the nucleus are shown in detail in the *Inset*. Blue, nucleus; orange, nucleolus; gray, mitochondria; yellow, vacuole; green, lipid bodies. (Scale bar, 1.0 μm).

CELL BIOLOGY

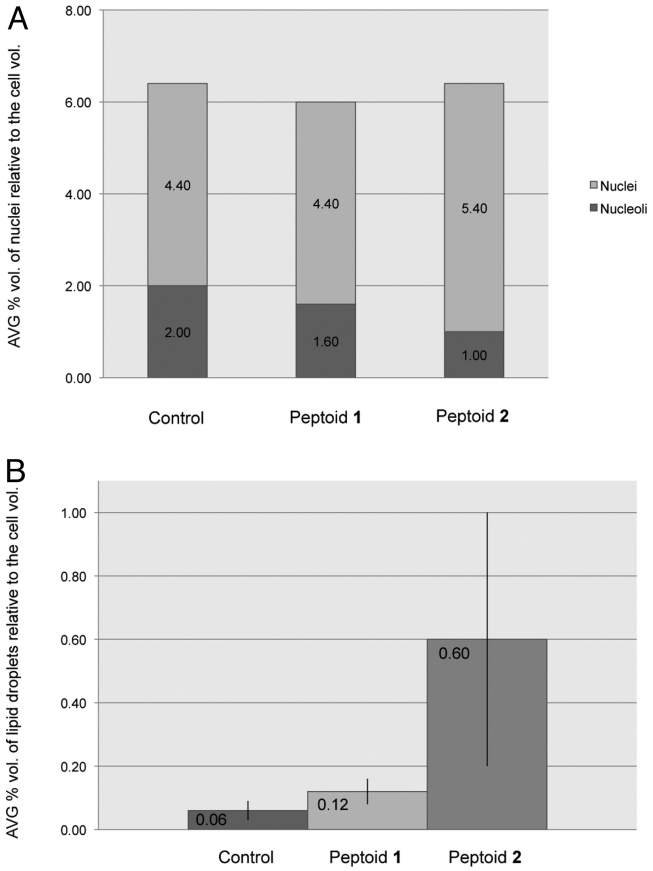

Fig. 4. Effect of peptoid treatment on selected organelle volumes. (*A*) Average percentage volume of the nucleus relative to the cell volume in control and peptoid treated cells. (*B*) Volume of lipid droplets in control and peptoid treated cells. The percentage relative value was calculated from the volume of each organelle divided by its cell volume. The error bars represent SD.

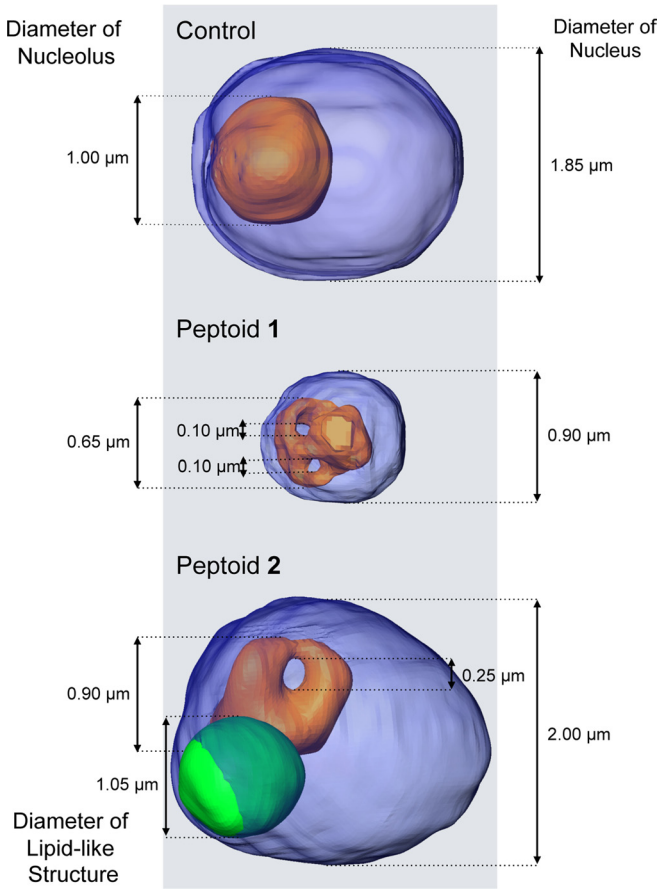

Fig. 5. Dimensions of nuclei, nucleoli, and a lipid-like structure shown in Fig. 3. Blue, nucleus; orange, nucleolus; green, lipid body.

bedded inside the nucleus of peptide 2 treated cells (Fig. 3*G*). These structures had LAC values in the range of those measured for lipid bodies, leading us to assign them accordingly. This observation was characteristic of virtually all cells treated with peptoid 2.

Discussion

Soft X-ray tomography is distinguishable from peer imaging techniques by the capacity to image fully hydrated eukaryotic cells in excess of 10 μm thick and do so without the use of stains or other contrast enhancing agents. Consequently, cells are imaged close to their native state.

Segmented reconstructions of *C. albicans* cells with yeast-like phenotype showed the mitochondria to be long, branched structures that surrounded both the nucleus and a single vacuole. The nucleus, nucleolus, and vacuole were approximately spherical, and organized as expected from studies using other imaging modalities. In hyphal cells, we observed a large population of discrete mitochondria localized at the tip region. This organization may be due to the large energy requirement for hyphal extension. However, the fragmented form of the mitochondria could also be the consequence of cell stress, because it is known that subcellular elements in the hyphal tip region are susceptible to any environmental change (33).

Segmented reconstructions of cells treated with peptoid 2 showed a number of clear differences with control cells, in particular in the nuclear region. The most striking of which are dense bodies observed to be embedded inside the nucleus (Figs. 3*G* and 5). Based on the measured LAC values and the shape of these objects, we surmise that these bodies are composed of lipids, or lipid-like, molecules. A similar report of enlarged lipid-droplets was described in *Saccharomyces cerevisiae* mutant cells, where a functional homologue of human seipin was deleted (32, 34). To our knowledge, this is the first observation of large lipid-like structures being embedded in the nucleus of *C. albicans*. The other striking feature visualized in the reconstructions of peptoid treated cells was the structure of the nucleoli. In all cases, the nucleoli in peptoid treated cells appear to contain one or more holes that pass completely through the organelle. Peptoid 2 treatment led to a single hole being present in the nucleoli, whereas peptoid 1 treatment resulted in nuclei that contained two such voids (Fig. 5) in all of the cells imaged. Again, the function, consequences, and underlying reason for these structural features remains an open question. It should also be stressed again that this type of observation could not have been made using diffraction limited fluorescence microscopy.

In all of the peptoid treated cells, the major phenotypic features displayed in Fig. 3 remained constant. Therefore, it is reasonable to speculate that these morphological changes have underlying functional consequences. These features could represent the stress response to peptoid treatment. Recent studies suggest that the nucleolus not only functions as the site for ribosome synthesis, but also has a key role in cell stress sensing. For example, under stress conditions, mammalian cells increase the level of tumor suppressor, p53, which leads to inhibition of Pol I transcription and altered nucleolus morphology (35–37). Although this work was not focused on the functional consequences of this structural arrangement, it is likely that the

application of antifungal peptoids led to this, or similar phenomena, suggesting that these mechanisms are suitable for therapeutic targeting.

In previous work by Isola et al. (31), the effects of salivary Histatin, an AMP, on *C. albicans* cells were imaged using transmission electron microscopy (TEM) and high-resolution scanning electron microscopy (HRSEM) (31). A number of Histatin-induced alterations in *C. albicans* cell structure were reported, such as the appearance of electron-dense bodies (thought to be mitochondrial in origin), membrane and organelle disarrangement, and the appearance of structures resembling autophagosomes. However, there was no clear indication of specific biochemical mechanism by which Histatin may function.

Developing new pharmaceuticals, such as antifungal drugs, is costly and unpredictable. Despite the availability of advanced research technologies, such as combinatorial chemistry and high-throughput screening methods, it still costs more than $1 billion to bring a new prescription drug to the market (8). The combination of high spatial resolution, together with a contrast mechanism that retains and reveals subtle features in cells, make soft X-ray tomography well suited to visualizing the consequences of treating cells with candidate drug molecules. The utility of the technique will increase in the near future, now that it is possible to carry out correlated high-aperture cryogenic fluorescence microscopy and soft X-ray tomography on the same specimen (16).

Materials and Methods

Strains, Cell Cultures, and Growth Conditions. *C. albicans* (wild-type strain 26555) was obtained from ATCC and grown at 26 °C on ATCC medium No.200 that contains 0.3% (wt/vol) yeast extract, 0.3%(wt/vol) malt extract, 0.5% (wt/vol) peptone, 1% (wt/vol) dextrose, and 2% (wt/vol) agar. Cell cultures were freshly prepared from these plates (one colony in 5 mL of liquid medium) and grown on a rotary shaker maintained at appropriate temperature overnight (OD = 1.5∼2.5). The phenotype was switched by modifying the growth conditions, as described in ref. 1.

Peptoid Treatment. Peptoids were synthesized as previously reported (20, 22). Liquid culture media containing overnight-cultured cells (100:1) and appropriate concentrations of peptoids were placed on the rotary shaker at 37 °C (t = 0). At this temperature, tube-like structures of *C. albicans* cells were induced. OD measurements were done every 30 min for 3 h (OD = ≈0.5). OD readings at 600 nm were performed on a Beckman DU640 spectrophotometer (Beckman Coulter) with a blank (i.e., appropriate concentrations of peptoids in liquid media).

Soft X-Ray Tomography. X-ray datasets were collected using the XM-2 soft X-ray microscope operated by the National Center for X-ray Tomography (http://ncxt.lbl.gov) at the Advanced Light Source (http://www.als.lbl.gov) of Lawrence Berkeley National Laboratory (LBNL). XM-2 is equipped with Fresnel zone plate based condenser and objective lenses (made by the Center for X-ray Optics, LBNL) and is specifically designed to investigate biological samples at cryogenic temperatures. For soft X-ray tomography, cells were rapidly transferred from their growth media to thin-walled glass capillaries, and immediately flash frozen in a cryogenic gas stream (13). No additional staining procedures were used. Imaging was performed with the specimens in an atmosphere of liquid nitrogen cooled helium gas at all times. For each dataset, 90 projection images were collected sequentially around a rotation axis in 2° increments to give a total rotation of 180°; the microscope was equipped with a resolution defining 50-nm objective lens. An exposure time of between 150 and 300 ms was used (depending on synchrotron ring current). Manual alignment of images, based on fiducial markers, was performed using the IMOD package (38). Tomographic reconstructions were calculated using iterative reconstruction methods (39–41).

Calculation of LACs and Manual Segmentation. Reconstructed cells were segmented into subvolumes that have similar LACs. The LAC for each voxel was measured directly from the experimental data. The absorption of soft X-rays follows Beer's Law, and therefore, is concentration and molecular species dependent. In the case of isolated biomolecules, the LAC can be measured experimentally or easily calculated according to the chemical composition of the specimen. For example, ice was calculated to have a LAC of 0.109 μm^{-1}, whereas a model protein with the chemical composition $C_{94}H_{139}N_{24}O_{31}S$ has a LAC of 1.35 μm^{-1} (19). The situation becomes more complex in the context of 50-nm voxels in a reconstruction of a cell. In this case, each voxel will almost certainly contain a mixture of biomolecules (lipids, protein, water, etc.). Therefore, the LAC for a segmented organelle is a measure of the overall biochemical composition. As can be seen from the reconstructed, unsegmented cell volumes (Fig. 1 *A*, *C*, and *E*) organelles have a relatively consistent LAC value, and therefore, are easily identifiable compared with other components in the cell (i.e., the nucleolus is readily distinguishable from the nucleus, lipid-dense bodies from the cytosol, etc.). Manual segmentation, measurements of voxel values to calculate LACs, and the creation of movies were all carried out using the Amira software package (Mercury Computer Systems).

Statistical Analysis of Autosegmented Data. Automatic segmentation was done using ITK-Snap V1.6.0.1 software (http://www.itksnap.org/pmwiki/pmwiki.php) (42), along with ImageJ 1.42k (http://rsbweb.nih.gov/ij/). ImageJ was used to reduce the noise from the data reconstructed by filtered back projection (39). Cells and lipid droplets were automatically segmented based on the threshold with corresponding LAC voxel values shown in Table S1; nucleoli and nuclei were semiautomatically segmented by the active contour method (42). All of the segmented volumes were smoothed by 3D median filtering, and all volumes with a voxel value of 5 or higher were included in the results.

ACKNOWLEDGMENTS. We thank Zeny Serrano for her skillful assistance with cell culture and peptoid treatment; Drs. Weiwei Gu and Dula Parkinson for assistance in the processing and alignment of the projection images and in the calculation of the tomographic reconstructions; and Tyler M. Miller for help with the peptoid synthesis. This work was funded by the Department of Energy Office of Biological and Environmental Research Grant DE-AC02-05CH11231, the National Institutes of Health (NIH) National Institute for Allergy and Infectious Diseases Grant GM072666, and the NIH National Center for Research Resources Grant RR019664.

1. Sudbery P, Gow N, Berman J (2004) The distinct morphogenic states of *Candida albicans*. *Trends Microbiol* 12:317–324.
2. Ashman RB, et al. (2004) Innate versus adaptive immunity in *Candida albicans* infection. *Immunol Cell Biol* 82:196–204.
3. Monk BC, Goffeau A (2008) Outwitting multidrug resistance to antifungals. *Science* 321:367–369.
4. Rappleyel CA, Goldman WE (2008) Fungal stealth technology. *Trends Immunol* 29:18–24.
5. Enoch DA, Ludlam HA, Brown NM (2006) Invasive fungal infections: A review of epidemiology and management options. *J Med Microbiol* 55:809–818.
6. Richardson M, Lass-Florl C (2008) Changing epidemiology of systemic fungal infections. *Clin Microbiol Infect* 14:5–24.
7. Wey SB, Mori M, Pfaller MA, Woolson RF, Wenzel RP (1988) Hospital-acquired candidemia. The attributable mortality and excess length of stay. *Arch Intern Med* 148:2642–2645.
8. Bullen A (2008) Microscopic imaging techniques for drug discovery. *Nat Rev Drug Discov* 7:54–67.
9. Hood L, Perlmutter RM (2004) The impact of systems approaches on biological problems in drug discovery. *Nat Biotechnol* 22:1215–1217.
10. Lang P, Yeow K, Nichols A, Scheer A (2006) Cellular imaging in drug discovery. *Nat Rev Drug Discov* 5:343–356.
11. Gu WW, Etkin LD, Le Gros MA, Larabell CA (2007) X-ray tomography of Schizosaccharomyces pombe. *Differentiation* 75:529–535.
12. Larabell CA, Le Gros MA (2004) X-ray tomography generates 3-D reconstructions of the yeast, *Saccharomyces cerevisiae*, at 60-nm resolution. *Mol Biol Cell* 15:957–962.
13. Le Gros MA, McDermott G, Larabell CA (2005) X-ray tomography of whole cells. *Curr Opin Struct Biol* 15:593–600.
14. Parkinson DY, McDermott G, Etkin LD, Le Gros MA, Larabell CA (2008) Quantitative 3-D imaging of eukaryotic cells using soft X-ray tomography. *J Struct Biol* 162:380–386.
15. Leis A, Rockel B, Andrees L, Baumeister W (2009) Visualizing cells at the nanoscale. *Trends Biochem Sci* 34:60–70.
16. Le Gros MA, McDermott G, Uchida M, Konechel CG, Larabell CA (2009) High aperture cryogenic light microsocpy. *J Microsc* 235:1–8.
17. Chao WL, Harteneck BD, Liddle JA, Anderson EH, Attwood DT (2005) Soft X-ray microscopy at a spatial resolution better than 15nm. *Nature* 435:1210–1213.
18. Attwood DT (1999) *Soft X-Rays and Extreme Ultraviolet Radioation: Principles and Applications* (Cambridge Univ Press, Cambridge, UK), p 470.
19. Weiss D, et al. (2000) Computed tomography of cryogenic biological specimens based on X-ray microscopic images. *Ultramicroscopy* 84:185–197.
20. Zasloff M (2002) Antimicrobial peptides of multicellular organisms. *Nature* 415:389–395.

21. Bessalle R, Kapitkovsky A, Gorea A, Shalit I, Fridkin M (1990) All-D-magainin: Chirality, antimicrobial activity and proteolytic resistance. *FEBS Lett* 274:151–155.
22. Latham PW (1999) Therapeutic peptides revisted. *Nat Biotechnol* 17:755–757.
23. Zuckermann RN, Kerr JM, Kent SBH, Moost WH (1992) Efficient Method for the Preparation of Peptoids [Oligo(N-substituted glycines)] by Submonomer Solid-Phase Synthesis. *J Am Chem Soc* 114:10646–10647.
24. Miller SM, et al. (1995) Comparison of the Proteolytic Susceptibilities of Homologous L-Amino Acid, D-Amino Acid, and N-Substituted Glycine Peptide and Peptoid Oliogmers. *Drug Devel Res* 35:20–32.
25. Chongsiriwatana NP, et al. (2008) Peptoids that mimic the structure, function, and mechanism of helical antimicrobial peptides. *Proc Natl Acad Sci USA* 105:2794–2799.
26. Patch JA, Barron AE (2003) Helical Peptoid Mimics of Magainin-2 Amide. *J Am Chem Soc* 125:12092–12093.
27. Makovitzki A, Avrahami D, Shai Y (2006) Ultrashort antibacterial and antifungal lipopeptides. *Proc Natl Acad Sci USA* 103:15997–16002.
28. Shai Y (2002) Mode of Action of Membrane Active Antimicrobial Peptides. *Biopolymers* 66:236–248.
29. Morton CO, et al. (2007) Global phenotype screening and transcript analysis outlines the inhibitory mode(s) of action of two amphibian-derived, alpha-helical, cationic peptides on *Saccharomyces cerevisiae*. *Antimicrob Agents Chemother* 51:3948–3959.
30. Riquelme M, Roberson RW, McDaniel DP, Bartnicki-Garcia S (2002) The effects of ropy-1 mutation on cytoplasmic organization and intracellular motility in mature hyphae of Neurospora crassa. *Fungal Genet Biol* 37:171–179.
31. Isola R, Isola M, Conti G, Lantini MS, Riva A (2007) Histatin-induced alterations in *Candida albicans*: A microscopic and submicroscopic comparison. *Microsc Res Tech* 70:607–616.
32. Fei W, et al. (2008) Fld1p, a functional homologue of human seipin, regulates the size of lipid droplets in yeast. *J Cell Biol* 180:473–482.
33. Szeghalmi A, Kaminskyj S, Gough KM (2007) A synchrotron FTIR microspectroscopy investigation of fungal hyphae grown under optimal and stressed conditions. *Anal Bioanal Chem* 387:1779–1789.
34. Ceelen H, et al. (1995) Bovine Somatotropin and the Regulatory Process for Veterinary Drug Approval - Open-Letter. *Can Vet J* 36:595–596.
35. Mayer C, Grummt I (2005) Cellular stress and nucleolar function. *Cell Cycle* 4:1036–1038.
36. Olson MO, Dundr M (2005) The moving parts of the nucleolus. *Histochem Cell Biol* 123:203–216.
37. Lo SJ, Lee CC, Lai HJ (2006) The nucleolus: Reviewing oldies to have new understandings. *Cell Res* 16:530–538.
38. Kremer JR, Mastronarde DN, McIntosh JR (1996) Computer visualization of three-dimensional image data using IMOD. *J Struct Biol* 116:71–76.
39. Mastronarde DN (1997) Dual-axis tomography: An approach with alignment methods that preserve resolution. *J Struct Biol* 120:343–352.
40. Erdogan H, Fessler JA (1999) Ordered subsets algorithms for transmission tomography. *Phys Med Biol* 44:2835–2851.
41. Stayman JW, Fessler JA (2000) Regularization for uniform spatial resolution properties in penalized-likelihood image reconstruction. *IEEE Trans Med Imaging* 19:601–615.
42. Yushkevich PA, et al. (2006) User-guided 3D active contour segmentation of anatomical structures: Significantly improved efficiency and reliability. *NeuroImage* 31:1116–1128.